Structural correlation with the Griffiths phase in disordered magnetic systems

Krishanu Ghosh,[1,2] Chandan Mazumdar,[3] R. Ranganathan,[3] S. Mukherjee,[1] and Molly De Raychaudhury[4]

[1]*Department of Physics, The University of Burdwan, Golapbag, Bardhaman 713104, West Bengal, India*

[2]*Department of Physics, P. C. Vigyan College, Kathari Bag Road, Chapra 841301, Bihar, India*

[3]*Condensed Matter Physics Division, Saha Institute of Nuclear Physics, 1/AF, Bidhannagar, Kolkata 700064, India*

[4]*Department of Physics, West Bengal State University, Barasat, Kolkata 700126, India*

(Received 14 June 2018; revised manuscript received 27 September 2018; published 16 November 2018)

In this work we report detailed experimental results and band structure calculations to establish a subtle link between the crystal structure and Griffiths phase (GP) behavior for the geometrically frustrated intermetallic $GdM_xSn_{2-\delta}$ (M = Co, Ni, Cu; $0 < x < 1, 0 \leqslant \delta \leqslant 0.22$) compounds. The crystal structure analysis through powder x-ray diffraction patterns reveals that the atomic positions of the M atoms in the GP analogs are slightly displaced in comparison to those of non-GP members of this series. Further, the band structure calculation shows that this slightly differing atomic position of M atoms results in narrowing in M d bands and the ferromagnetic clusters centered on the T atoms are responsible for GP behavior. This effect is insignificant in non-GP members.

DOI: 10.1103/PhysRevB.98.184419

I. INTRODUCTION

Crystal structures often play an important role in various magnetic properties of systems, viz., multiferroic behavior, giant magnetocaloric nature, magnetism in semiconductors, colossal magnetoresistance, etc. [1–5]. This also includes the Griffiths phase (GP), which was first proposed theoretically by Griffiths [6] in connection to the Ising ferromagnetic (FM) system, where all the lattice sites are occupied by magnetic spins (the probability of occupancy $p = 1$) having nearest-neighbor exchange interactions J and exhibiting a long-range FM ordering temperature $T_C^{\text{undiluted}}$. When such a system is diluted randomly ($p < 1$), the nearest-neighbor exchange interactions become either J or zero depending on the presence or absence of spins, respectively. This results in weakening the cooperative interactions among magnetic spins, thus reducing the magnetic transition temperature T_C for the diluted system ($T_C < T_C^{\text{undiluted}}$). Below a certain critical concentration $p < p_0$ (p_0 is the critical percolation probability), the system fails to show any long-range magnetic order. In the intermediate range ($p_0 < p < 1$) the system contains large clusters, as a result of which it exhibits nonanalytical behavior of thermodynamic properties in the temperature region $T_C < T < T_C^{\text{undiluted}}$. Such a disorder-driven magnetic phase, intermediate between the perfectly ordered magnetic state and completely disordered paramagnetic state, is known as the Griffiths phase [6], and the temperature $T_C^{\text{undiluted}}$ is known as the Griffiths temperature T_G. The concept was later generalized for any arbitrary bond probability distribution, where T_G is determined by the highest ordering temperature allowed by the distribution [7].

Experimentally, the GP is often found in systems with quenched disorder and/or competing magnetic interactions, e.g., different manganites, semiconductors, oxides, intermetallics, etc. Chemical substitution is one of the simplest ways of achieving the required disorder in an otherwise magnetically ordered system, e.g., in many manganites [8–14], $R_5(Si_xGe_{1-x})_4$ (R = rare earth) intermetallics [1,15], etc. On the other hand, properties like microtwinning, competing magnetic interactions, etc., can also be found to be responsible for inducing GP in chemically undisturbed compounds, viz., R_5Ge_4 [1,16], Ca_3CoMnO_6 [17], etc. The observed GP behavior in the layered compound R_5Ge_4 has been argued to be due to local crystallographic disorder, originating from competing interlayer and intralayer magnetic exchange interactions [1,16,18]. In the case of the geometrically frustrated magnetic (GFM) system Ca_3CoMnO_6 a particular magnetic spin arrangement has been argued to be responsible for the GP behavior [17]. A very similar spin arrangement was previously reported in another GFM series of intermetallic compounds, RFe_xSn_2 (R = Tb–Tm) [19]. These compounds crystallize in the defect orthorhombic $CeNiSi_2$-type crystal structure [20] where transition-metal atoms are randomly distributed [21,22]. Interestingly, as in the case of $R_5(Si_xGe_{1-x})_4$-type compounds, atoms in the $CeNiSi_2$-type crystal structure are arranged in layers stacked perpendicular to the b axis [21]. We previously reported $GdFe_{0.17}Sn_{2-\delta}$ forming in the $CeNiSi_2$-type crystal structure to be a rare example of an intermetallic GFM compound that also exhibits GP behavior [23].

To understand the origin of the GP in $GdFe_{0.17}Sn_{2-\delta}$, it is essential to study the magnetic properties of other members of the $GdM_xSn_{2-\delta}$ (M = transition metal) series of compounds and compare their properties. In this work, we report the interrelation between the structural parameters and GP behavior in the $GdM_xSn_{2-\delta}$ (M = Co, Ni, Cu) series of compounds. Our band structure analysis explains the origin of GP vis-à-vis the modifications of crystal structure in the compounds studied here. We focus on only the Gd-based system due to its negligible magnetic anisotropy [24].

II. METHODS

A number of polycrystalline compounds with the nominal compositions $GdM_{0.17}Sn_{2-\delta}$ (M = Co, Ni, and Cu),

 ©2018 American Physical Society

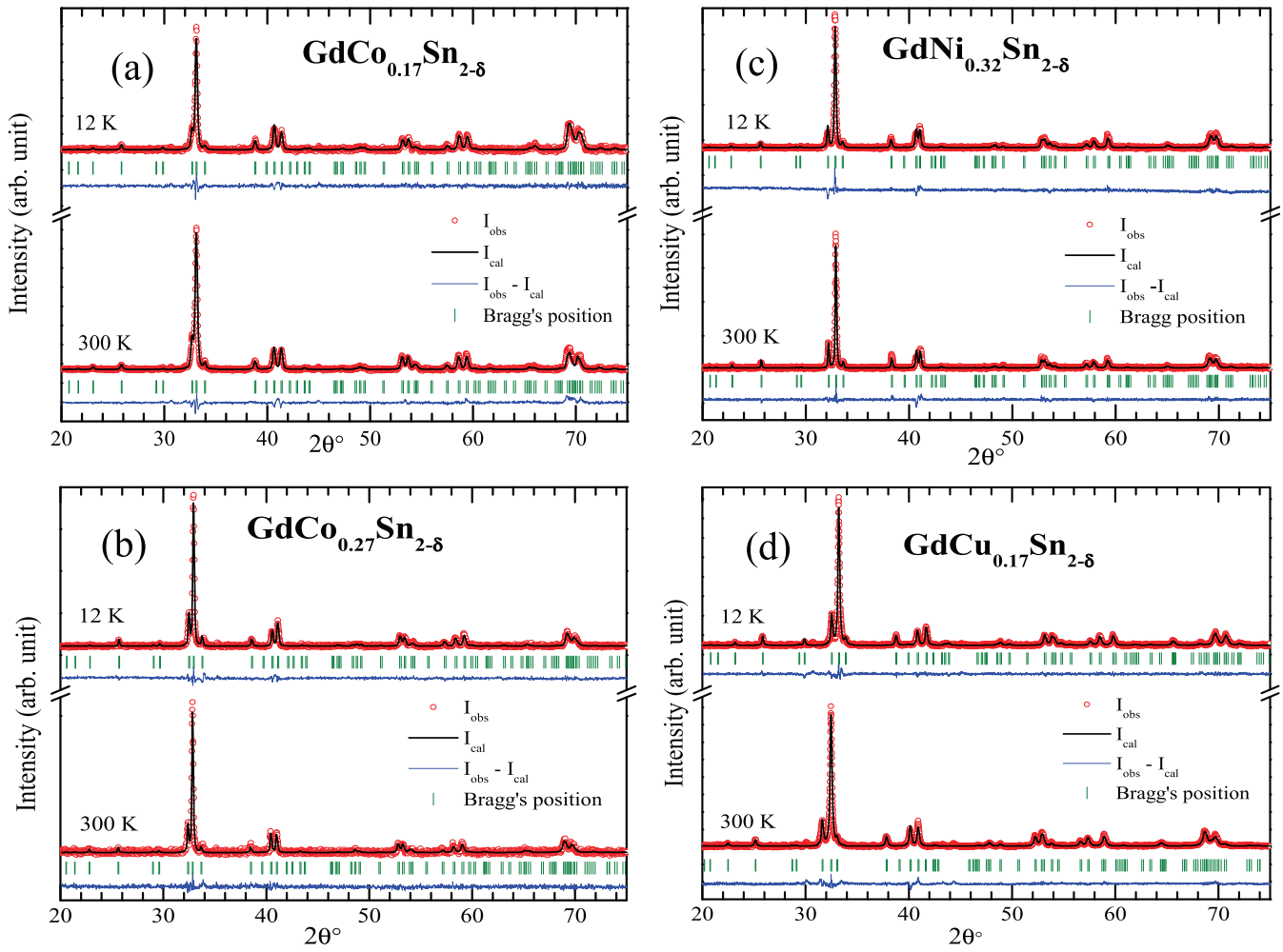

FIG. 1. XRD patterns measured at 12 K (top) and at room temperature (bottom) for (a) $GdCo_{0.17}Sn_{2-\delta}$, (b) $GdCo_{0.27}Sn_{2-\delta}$, (c) $GdNi_{0.32}Sn_{2-\delta}$, and (d) $GdCu_{0.17}Sn_{2-\delta}$.

$GdCo_{0.27}Sn_{2-\delta}$, and $GdNi_{0.32}Sn_{2-\delta}$ were synthesized with the arc-melting process on a water-cooled copper hearth in a flowing-argon atmosphere. For better homogeneity, the samples were remelted four or five times. The weight loss of the sample during this process was found to be less than 0.5%. The resultant ingots were then wrapped in Ta foil and annealed under vacuum in sealed quartz tubes at 800 °C for 15 days. Powder x-ray diffraction (XRD) measurements were performed in the temperature range of 12–300 K using an 18-kW rotating anode diffractometer (model: TTRAX-III, Rigaku Corp., Japan). These data were analyzed through the Rietveld refinement analysis using FULLPROF software [25]. The spatial homogeneity and elemental composition of the compounds were checked with a scanning electron microscope (SEM; EVO 18, Carl Zeiss, Germany) and energy dispersive x-ray analysis (EDAX; EDAX, United States), respectively. Heat capacity (in the absence of external magnetic field) and magnetic measurements were performed in the temperature range of 4–300 K using a commercial physical property measurement system Evercool-II and superconducting quantum interference device vibrating-sample magnetometer (Quantum Design, United States). The molar magnetic susceptibility and heat capacity of the compounds were estimated by considering the chemical composition determined from Rietveld analysis.

III. RESULTS AND DISCUSSION

In our attempt to understand the origin of the GP in $GdFe_{0.17}Sn_{2-\delta}$, we synthesized different members of the intermetallic series $GdM_xSn_{2-\delta}$ (M = Co, Ni, Cu). Out of these, the formation of $GdCo_{0.27}Sn_{2-\delta}$, $GdNi_{0.32}Sn_{2-\delta}$, and $GdCu_{0.17}Sn_{2-\delta}$ have been reported in the literature [22]. Additionally, we have also attempted to synthesize $GdCo_{0.17}Sn_{2-\delta}$ and $GdNi_{0.17}Sn_{2-\delta}$, of which the last composition could not be formed in a single phase. The room-temperature and low-temperature (12 K) XRD data of $GdCo_{0.17}Sn_{2-\delta}$, $GdCo_{0.27}Sn_{2-\delta}$, $GdNi_{0.32}Sn_{2-\delta}$, and $GdCu_{0.17}Sn_{2-\delta}$ are presented in Fig. 1. The XRD peaks of all these compounds can be indexed considering the $CeNiSi_2$-type orthorhombic structure (space group *Cmcm*), where all the atoms occupy different 4*c* (0, *y*, 0.25) Wyckoff positions [20]. The structural parameters of all these compounds found from the Rietveld refinement of powder XRD data recorded at 300 K are presented in Table I. Except for the lattice parameters of the compound $GdCo_{0.17}Sn_{2-\delta}$ (for which no published data is available), all

TABLE I. Lattice parameters and elemental compositions (from XRD analysis) and magnetic data of $GdM_xSn_{2-\delta}$ compounds.

	Nominal composition				
	$GdFe_{0.17}Sn_{2-\delta}$ [23]	$GdCo_{0.27}Sn_{2-\delta}$	$GdCo_{0.17}Sn_{2-\delta}$	$GdNi_{0.32}Sn_{2-\delta}$	$GdCu_{0.17}Sn_{2-\delta}$
Full Rietveld analysis	$GdFe_{0.19}Sn_{1.93}$	$GdCo_{0.28}Sn_{1.78}$	$GdCo_{0.20}Sn_{1.97}$	$GdNi_{0.28}Sn_{2.00}$	$GdCu_{0.16}Sn_{1.87}$
a (Å)	4.443(1)	4.442(1)	4.436(1)	4.427(1)	4.433(1)
b (Å)	16.43(1)	16.50(1)	16.43(1)	16.66(1)	16.68(1)
c (Å)	4.371(1)	4.385(1)	4.363(1)	4.388(1)	4.354(1)
v (Å^3)	319.23(9)	321.39(9)	317.99(5)	323.52(4)	322.01(5)
y_{Gd}	0.096(1)	0.100(1)	0.098(1)	0.101(1)	0.100(1)
y_M	0.385(9)	0.385(6)	0.297(3)	0.298(2)	0.318(2)
$y_{Sn(1)}$	0.439(1)	0.437(1)	0.436(1)	0.438(1)	0.439(1)
$y_{Sn(2)}$	0.749(1)	0.744(1)	0.748(1)	0.749(1)	0.748(1)
R_{Bragg} (%)	7.14	14.9	11.7	9.67	9.25
R_f (%)	9.68	19.3	13.9	10.2	11.0
T_N (K)	16.5	16.5	16.5	13.8	24.0
T_G (K)	32	32			
θ_p (K)	−59	−45	−54	−49	−62
μ_{eff} (units of μ_B)	8.19	8.13	8.03	8.02	8.01
$f = \lvert\theta_p\rvert / T_N$	3.6	2.7	3.3	3.6	2.6

the other values are in agreement with earlier published results [22]. The full Rietveld analysis of the XRD patterns reveals the presence of noticeable vacancies at the Sn sites ($0 \leqslant \delta \leqslant 0.22$) in some of the compounds (Table I). Such Sn deficiencies were reported earlier for most of the $CeNiSi_2$-type stannides [21,26], e.g., $GdFe_{0.19}Sn_{1.93}$ [23], $RM_{0.24}Sn_{1.79}$ (M = Fe, Mn) [21], $CeMn_{0.4}Sn_{1.9}$ [21], etc. Backscattered electron (BSE) imaging and EDAX analysis were also performed for $GdCo_{0.17}Sn_{2-\delta}$ and $GdCo_{0.27}Sn_{2-\delta}$ (Fig. 2). Both compounds were found to be essentially of a single-phase nature. The average compositions obtained from EDAX analysis are $GdCo_{0.200(5)}Sn_{1.953(15)}$ and $GdCo_{0.308(8)}Sn_{1.816(15)}$ which were found to be close to those estimated from Rietveld analysis of XRD data for those two compounds. EDAX analysis of $GdFe_{0.17}Sn_{2-\delta}$ was reported earlier [23].

The dc magnetic susceptibility (M/H) measurements for all the compounds in both zero-field-cooled (ZFC; Fig. 3) and field-cooled (FC) configurations exhibit a well-defined peak at low temperatures, suggesting the antiferromagnetic (AFM) type of magnetic ordering (Table I). The long-range nature of the magnetic ordering was confirmed through zero-field heat capacity measurements (Fig. 3, inset). The effective magnetic moment per formula unit μ_{eff} and paramagnetic Weiss temperature θ_p, estimated from the inverse magnetic susceptibility in the high-temperature region, are listed in Table I. The estimated values of μ_{eff} are found to be close to that of free Gd^{3+} ions ($7.94\mu_B$). On the other hand, θ_p values are found to be negative and large (Table I), similar to that observed earlier in the case of $GdFe_{0.17}Sn_{2-\delta}$ [23] and $GdCo_{0.4}Ge_2$ [27]. The frustration parameter, $f = |\theta_p|/T_N$, estimated from magnetic susceptibility data (Table I) is also found to be quite large, indicating a typical GFM nature [28]. Neutron diffraction experiments on structurally related compounds, RFe_xSn_2 (R = Tb–Tm, $0.1 < x < 0.15$), indicate that R atoms at the corners of trigonal prisms and/or tetrahedrons [19] are responsible for the GFM behavior. The magnetic structures for the Gd-based systems could not be checked directly due to the large neutron absorption cross section of Gd.

The inverse magnetic susceptibility, measured under low applied magnetic field H, however, deviates significantly

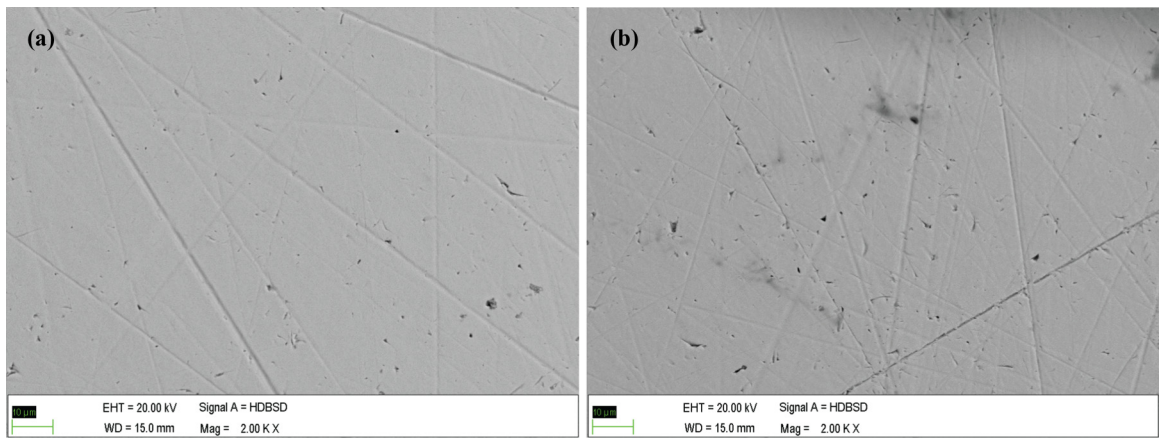

FIG. 2. SEM image in the BSE mode for (a) $GdCo_{0.17}Sn_{2-\delta}$ and (b) $GdCo_{0.27}Sn_{2-\delta}$.

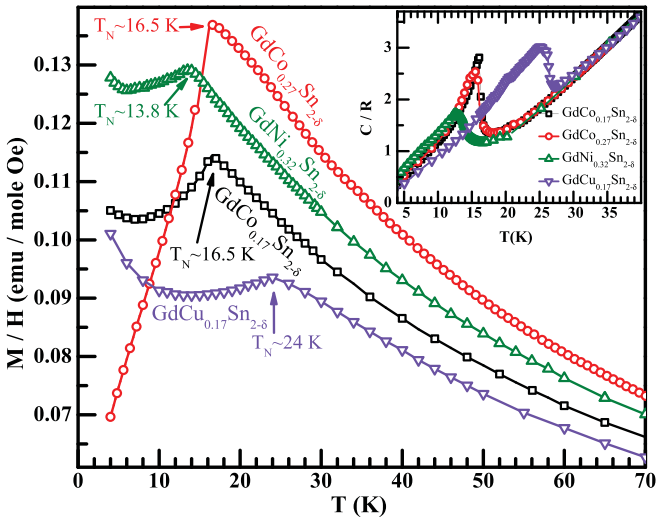

FIG. 3. Temperature dependence of the magnetic susceptibilities of $GdM_xSn_{2-\delta}$ (M = Co, Ni, and Cu) measured at 100 Oe magnetic field in the ZFC configuration. Inset: Temperature dependence of heat capacity of $GdM_xSn_{2-\delta}$ (M = Co, Ni, and Cu) in the absence of any externally applied magnetic field, plotted in units of the universal gas constant R.

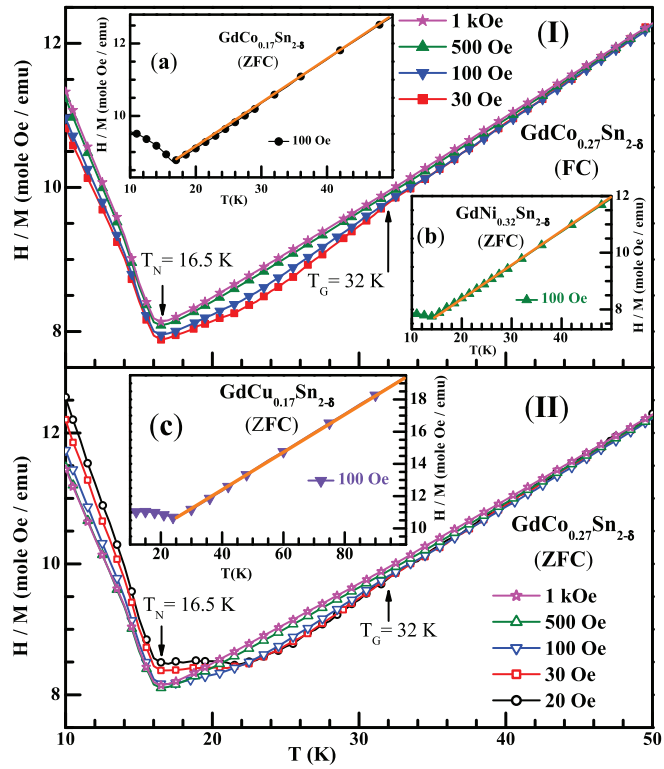

FIG. 4. Temperature dependence of the inverse magnetic susceptibilities of $GdCo_{0.27}Sn_{2-\delta}$ measured at different externally applied magnetic fields under FC (top) and ZFC (bottom) configurations during a warming cycle. Inset (a): Temperature dependence of the inverse magnetic susceptibilities of $GdCo_{0.17}Sn_{2-\delta}$ measured at H = 100 Oe in the ZFC configuration. Inset (b): Temperature dependence of the inverse magnetic susceptibilities of $GdNi_{0.32}Sn_{2-\delta}$ measured at H = 100 Oe in the ZFC configuration. Inset (c): Temperature dependence of the inverse magnetic susceptibilities of $GdCu_{0.27}Sn_{2-\delta}$ measured at H = 100 Oe in the ZFC configuration.

from the Curie-Weiss (CW) behavior below 32 K in the case of $GdCo_{0.27}Sn_{2-\delta}$ (Fig. 4). The nature of the deviation is found to be different in the FC and ZFC protocols, although in both cases, the extent of the deviation diminishes as H increases. In the FC protocol, the inverse susceptibility exhibits a downward deviation in the temperature range $T_N = 16.5\ \text{K} < T < T_G = 32\ \text{K}$. As H increases, the extent of the deviation decreases gradually. Above $H \geqslant 1$ kOe, the inverse susceptibility follows CW behavior down to T_N (Fig. 4, top). This is the characteristic feature of the GP as reported previously in many systems [1,9–17,29,30], including isostructural $GdFe_{0.17}Sn_{2-\delta}$ [23]. We must note here that the magnetic susceptibility χ of the GP is generally known to follow the power law describing the Griffith singularity [31]

$$\chi^{-1} \propto \left(T - T_C^R\right)^{1-\lambda}, \tag{1}$$

where λ is the magnetic susceptibility exponent and T_C^R is the critical temperature of random ferromagnetic clusters where susceptibility tends to diverge. However, the limited range of the temperature region between T_N and T_G and the large negative value of θ_p of $GdCo_{0.27}Sn_{2-\delta}$ do not allow us to check the power law behavior. This was discussed in detail for isostructural $GdFe_{0.17}Sn_{2-\delta}$ [23]. The measurement in the ZFC protocol, additionally, exhibits a thermoremanence behavior, along with the GP feature in the same temperature range, $T_N < T < T_G$, observed in the FC measurement (Fig. 4, bottom). This thermoremanence behavior results from the intercluster interactions that hinder the magnetic response to the external magnetic field, reducing the value of χ with the lowering of temperature below 22 K (in 20 and 30 Oe field for $GdCo_{0.27}Sn_{2-\delta}$). As H increases, the strength of the thermoremanence diminishes gradually, and for a field larger than 100 Oe, ZFC and FC magnetizations exhibit similar temperature dependence. As in the case of the FC measurement, the ZFC measurement for $H \geqslant 1$ kOe exhibits CW behavior above T_N. Similar thermoremanence behavior in the ZFC case in the GP system was reported previously in the case of $GdFe_{0.17}Sn_{2-\delta}$ [23]. However, no such anomaly like a GP is seen in the case of $GdCo_{0.17}Sn_{2-\delta}$, $GdNi_{0.32}Sn_{2-\delta}$, and $GdCu_{0.17}Sn_{2-\delta}$ [Fig. 4, insets (a), (b), and (c)].

It is thus rather surprising that among all the $GdM_xSn_{2-\delta}$ (M = Co, Ni, and Cu; $0 < x < 1$) compounds studied here, only $GdCo_{0.27}Sn_{2-\delta}$ shows a GP. Even $GdCo_{0.17}Sn_{2-\delta}$, which is compositionally very close to $GdCo_{0.27}Sn_{2-\delta}$, fails to exhibit GP behavior. Generally, in rare-earth (R)-based intermetallic compounds, the magnetic interaction J is the Ruderman-Kittel-Kasuya-Yosida (RKKY) type and takes place between two localized $4f$ spins via conduction electrons. The sign and strength of the RKKY interaction essentially depend on the distances between the $4f$ spins [32]. Primarily, any variation between Gd-Gd distances in any one of these compounds may therefore result in different magnetic properties than the rest. To understand the origin of the GP in $GdCo_{0.27}Sn_{2-\delta}$, which is primarily a magnetic phenomenon, it is therefore essential to compare the atomic arrangements in the $CeNiSi_2$-type crystal structure for all the compounds studied here.

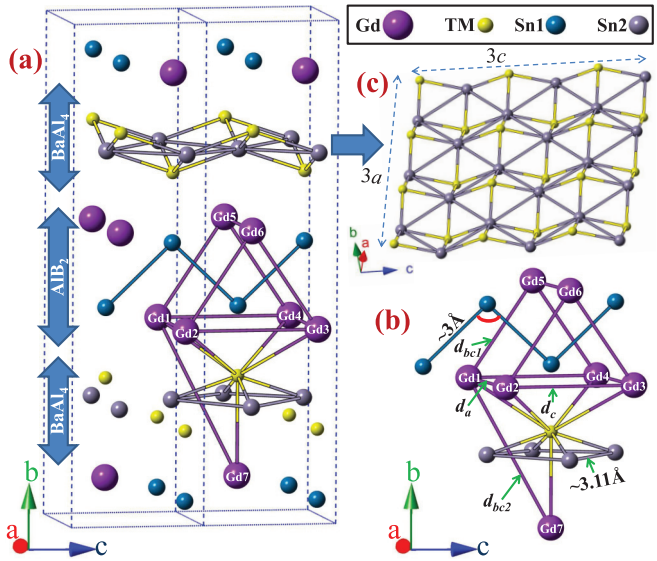

FIG. 5. (a) $CeNiSi_2$-type crystal structure of $GdM_xSn_{2-\delta}$ (M = Co, Ni, and Cu) compounds, showing intergrowth sequences of $BaAl_4$ and AlB_2-like slabs. (b) Part of the atomic arrangement in the crystal structure emphasizing different interatomic distances and angles. (c) $BaAl_4$ slab viewed approximately down the b axis, i.e., the planar square nets of 4(Sn2) capped alternatively above and below with M atoms.

The majority of the RM_xX_2 (M = transition metals, X = Si, Ge, Sn) type of compounds form in the well-known orthorhombic $CeNiSi_2$ structure type (space group *Cmcm*). Although all the atoms, viz., R, M, $X1$, and $X2$, occupy the same point group symmetry, 4c (0, y, 0.25) [20], the interelement cross-substitutional effect was reported to be negligible [33]. It was also reported that while those RM_xSi_2 types of compounds form in stoichiometric compositions, a large number of corresponding germanides and almost all the known stannides form with vacancies in transition-metal sites [22]. Additionally, the transition-metal concentration is found to be quite low for the stannides [22]. The $CeNiSi_2$-type structure itself may be considered as intergrowth of ternary $BaAl_4$ and binary AlB_2 slabs along the b axis [Fig. 5(a)] and may also be viewed as a partially filled version of the $ZrSi_2$ structure type (space group *Cmcm*) [21]. In the AlB_2 slab, the rare-earth atoms [Gd1 to Gd6 in Fig. 5(a)] are arranged in the shape of trigonal prisms. The four Gd atoms (Gd1 to Gd4) form the base of the prism in the ac plane [Fig. 5(a)], and the distances between Gd1-Gd2 (or Gd3-Gd4; assigned as d_a) and Gd1-Gd4 [or Gd2-Gd3; assigned as d_c; Fig. 5(b)] are the corresponding lattice parameters, a and c, respectively, of that compound. The Gd5 (or Gd6) atom completes the triangle of a face of the trigonal prisms [Fig. 5(a)] and is situated at a distance d_{bc1} from Gd1 [or Gd2; Fig. 5(b)]. Sn1 atoms are arranged in a zigzag chain passing through the trigonal prisms of Gd along the c axis [Fig. 5(a)]. The $BaAl_4$ slab contains planer square nets of four Sn2 atoms, alternatively capped above and below by the M atoms [Fig. 5(c)] [34]. The vacancies in the transition-metal sites that are found in $RM_xSn_{2-\delta}$ compounds generally influence this layer. It was argued that to stabilize the structure, the defects in the transition-metal sites introduce additional defects in the Sn site, randomly distributed over both slabs [35].

To compare the possible influence of relative atomic arrangements in GP and non-GP compounds of the $GdM_xSn_{2-\delta}$ series, one may consider an ideal pair to be $GdCo_{0.27}Sn_{2-\delta}$ (GP) and $GdCo_{0.17}Sn_{2-\delta}$ (non-GP) since both compounds consist of the same set of elements and form in the same crystal structure. The structural information used in this study was estimated from the powder XRD analysis, which yields the bond lengths and angles averaging over a large volume. The primary bond lengths that are important, viz., d_a, d_c, d_{bc1}, and d_{bc2} [Fig. 5(b)], are listed in Table II. The estimated values of the above parameters for $GdCo_{0.27}Sn_{2-\delta}$ and $GdCo_{0.17}Sn_{2-\delta}$ show no significant differences. The absence of any major differences in the arrangement of Gd ions in both $GdCo_{0.27}Sn_{2-\delta}$ and $GdCo_{0.17}Sn_{2-\delta}$ suggests that the different magnetic properties of the compounds must have an origin other than the one controlled by Gd-Gd distances. Since RKKY interaction is also controlled by the polarization of the conduction electrons, it is therefore essential to look for any possible difference in the arrangement of the M and Sn atoms, which should also contribute to the conduction electron density. We find no significant difference in the arrangement of Sn1 atoms in the zigzag chain, which have very similar bond lengths (∼3 Å) and similar bond angles (∼93°) for both the compounds.

However, a major structural difference indeed exists in the $BaAl_4$ slab of the GP compound $GdCo_{0.27}Sn_{2-\delta}$ and the non-GP compound $GdCo_{0.17}Sn_{2-\delta}$. Although in both compounds the square Sn2 nets appear to be rather similar, the relative positions of Co atoms with respect to the Sn2 net are found to be very different. This can be seen clearly from the estimated bond lengths and angles (Table III). One, however, may note here that these bond length values might not always represent the actual individual bond distances, but rather, they are the calculated bond lengths averaged over the entire volume. For systems with considerable M-site vacancies, the calculated M bond lengths from XRD analysis could turn out to be smaller than the sum of their individual ionic radii [21]. Similarly, in the present study, as we increase the Co content from 17% to

TABLE II. Bond lengths and bond angles (similarity).

Compound	d_a (Å)	d_c (Å)	d_{bc1} (Å)	d_{bc2} (Å)	Sn1-Sn1 (Å)	∠ Sn1-Sn1-Sn1 (deg)	Sn2-Sn2 (Å)
$GdFe_{0.17}Sn_{2-\delta}$	4.444	4.371	3.852	5.930	2.966	94.94	3.117
$GdCo_{0.27}Sn_{2-\delta}$	4.442	4.385	3.984	5.830	3.004	93.74	3.125
$GdCo_{0.17}Sn_{2-\delta}$	4.436	4.364	3.911	5.862	3.017	92.65	3.112
$GdNi_{0.32}Sn_{2-\delta}$	4.427	4.388	4.036	5.841	2.995	94.19	3.117
$GdCu_{0.17}Sn_{2-\delta}$	4.433	4.354	3.990	5.885	2.978	93.95	3.107

TABLE III. Bond lengths and bond angles (dissimilarity).

Compound	M-Sn1 (Å)	$\angle$ M-Sn2-M (deg)	$\angle$ Sn2-M-Sn1 (deg)
$GdFe_{0.17}Sn_{2-\delta}$	0.90	89.66	135.17
$GdCo_{0.27}Sn_{2-\delta}$	0.87	91.20	134.40
$GdCo_{0.17}Sn_{2-\delta}$	2.29	142.49	108.78
$GdNi_{0.32}Sn_{2-\delta}$	2.33	139.57	110.22
$GdCu_{0.17}Sn_{2-\delta}$	2.01	125.34	117.33

27%, there is a drastic reduction in the Co-Sn1 bond length, from 2.29 to 0.87 Å. This also affects the average values of the Co-Sn2-Co and Sn2-Co-Sn1 angles to a great extent, as the former angle reduces from 142.49° to 91.20°, and the latter correspondingly increases from 108.78° to 134.40° (Table III and Fig. 6). Therefore, the Co-Sn2 arrangement appears to be more distorted in the case of $GdCo_{0.27}Sn_{2-\delta}$ than $GdCo_{0.17}Sn_{2-\delta}$. A similar structural distortion may be visualized from the low-temperature atomic arrangements of isostructural $ErCo_{0.4}Ge_2$ in comparison to $ErCo_{0.47}Ge_2$ [27]. We must point out here that in the $CeNiSi_2$ type of crystal structure, $BaAl_4$ slabs are often found to be susceptible to deformation. For example, it was previously reported that $TbFe_{0.25}Ge_2$ exhibits a monoclinic distortion due to the modulation of the Ge2 net in the same $BaAl_4$ slab [34].

We thus see that the primary difference between the GP compound $GdCo_{0.27}Sn_{2-\delta}$ and the non-GP compound $GdCo_{0.17}Sn_{2-\delta}$ lies in the relative shape of the Co-4(Sn2) square pyramid. To check this hypothesis, we carried out crystal structure analysis of another GP compound, $GdFe_{0.17}Sn_{2-\delta}$, and other non-GP compounds, $GdNi_{0.32}Sn_{2-\delta}$ and $GdCu_{0.17}Sn_{2-\delta}$, belonging to the same crystal structure. The results are given in Tables II and III. We find that the shapes of the M-4(Sn2) square pyramids for GP compounds $GdCo_{0.27}Sn_{2-\delta}$ and $GdFe_{0.17}Sn_{2-\delta}$ appear to be very similar, which is quite different from the non-GP compounds $GdCo_{0.17}Sn_{2-\delta}$, $GdNi_{0.32}Sn_{2-\delta}$, and $GdCu_{0.17}Sn_{2-\delta}$. It therefore appears that the origin of the GP in these materials depends strongly on the atomic arrangement of M atoms.

In order to test the appropriateness of such a conjecture, we studied the effect of such a distortion in the local square pyramidal atomic arrangements through detailed band structure analysis. The primary objective of the study is to observe

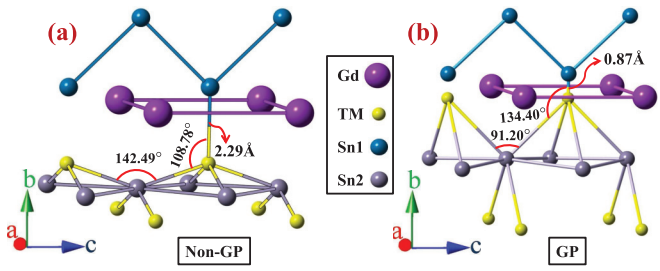

FIG. 6. Distances and angles between various atoms of (a) $GdCo_{0.17}Sn_{2-\delta}$, a representative of non-GP, and (b) $GdCo_{0.27}Sn_{2-\delta}$, a representative of GP, in $GdM_xSn_{2-\delta}$ (M = Fe, Co, Ni, and Cu; $0 < x < 1$).

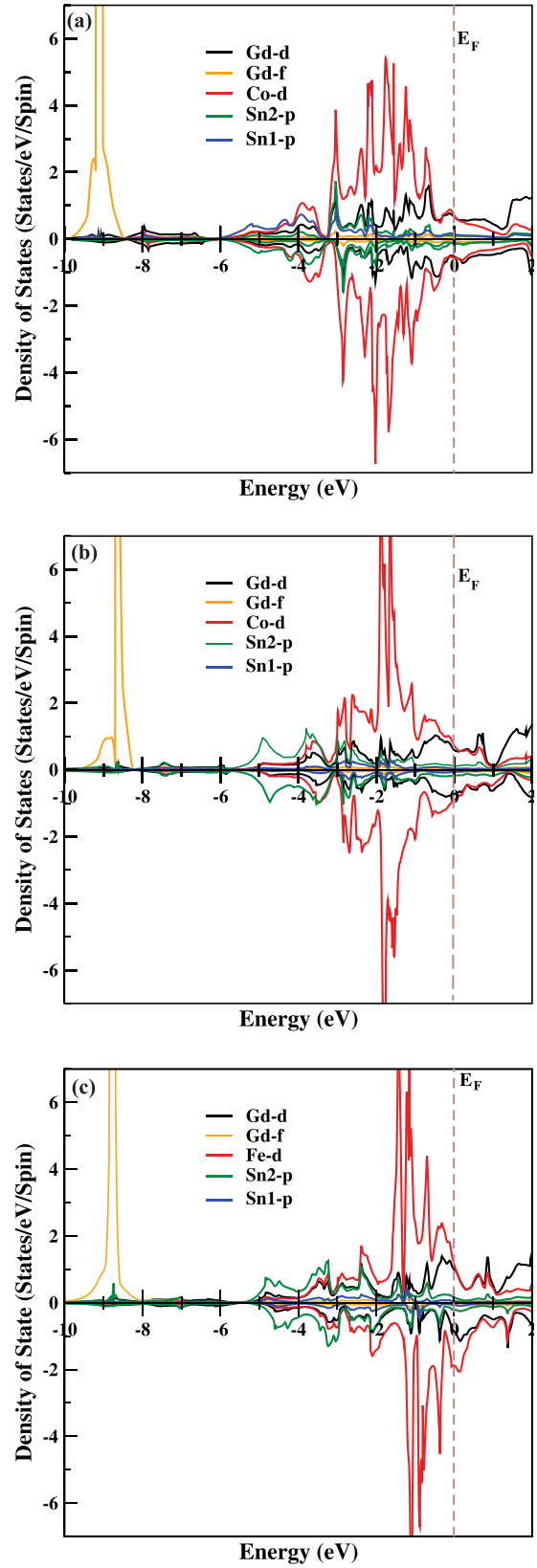

FIG. 7. Partial density of states (PDOS) for $GdCoSn_2$ using the structural parameters of (a) $GdCo_{0.17}Sn_{2-\delta}$ and (b) $GdCo_{0.27}Sn_{2-\delta}$. (c) PDOS for $GdFeSn_2$ using the structural parameters of $GdFe_{0.17}Sn_{2-\delta}$. E_F represents Fermi energy at 0 K.

the influence of M atoms on neighboring atoms. Accordingly, we approximated the defect composition as the stoichiometric $GdMSn_2$ with the lattice parameters and atomic coordinates of $GdCo_{0.27}Sn_{2-\delta}$/$GdFe_{0.17}Sn_{2-\delta}$/$GdCo_{0.17}Sn_{2-\delta}$ in the respective cases. $GdCo_{0.27}Sn_{2-\delta}$ is the representative of GP compounds, whereas $GdCo_{0.17}Sn_{2-\delta}$ is the representative non-GP compound. A similar approach was previously adopted for the calculation of electronic structures in the isostructural RLi_xSn_2 series of materials [35].

The spin-polarized density functional calculations were performed using the local-spin-density approximation + Hubbard U (LSDA + U) formalism [36] which included electronic correlations. The latter is particularly large in Gd 4f electrons and comparatively negligible among Co d electrons. In our calculation, we used the parameters Hubbard U = 8.0 eV and J = 1.2 eV for Gd 4f electrons [37], and the basis chosen was the linear muffin-tin orbital [38].

The resulting band structure of $GdCoSn_2$ yields the effective magnetic moment μ_{eff} per formula unit as $8.25\mu_B$ and $8.28\mu_B$ for the crystal structure without and with the pyramidal distortion, respectively. This slight enhancement of μ_{eff} for the compound with a distorted pyramidal structure is also evident from the experimentally observed enhancement of μ_{eff} from $8.03\mu_B$ for $GdCo_{0.17}Sn_{2-\delta}$ to $8.13\mu_B$ for $GdCo_{0.27}Sn_{2-\delta}$ (Table I). The spin moment of the Co d electrons not only changes but also reorients more along the spin polarization of the Gd d and Gd f electrons as distortion in its environment sets in. This change in the behavior of the Co d electrons and hence their spin moment is also evident from the reduced Co d-band width in the calculated partial density of states (PDOS) [Figs. 7(a) and 7(b)]. It seems that the distortion causes the narrowing of the Co d band, which then starts dominating over the Gd d states at the Fermi level. This altered hybridization of Gd d states with localized Co d electrons at the Fermi level causes the overall localization of the conduction electrons which were predominantly derived from delocalized Gd d electrons in the undistorted structure. It is understandable that dilute Co doping as in the corresponding nonstoichiometric compounds may lead to a larger spin moment of Co ions, and hence, the real picture can be much more complex.

Since the RKKY exchange mechanism in rare-earth-based compounds is mediated by the conduction electrons, the partial localization of the Gd d conduction electrons should modify this magnetic interaction too. The calculated PDOS suggests that the RKKY-driven AFM exchange interaction takes place in the Gd-Sn1 quasiplane through the Co ion. In the synthesized compounds, Co doping should disrupt the RKKY exchange interaction among the Gd 4f electrons. According to Sobota *et al.* [39], localization due to doping in RKKY systems helps them to achieve a rare disordered configuration that builds up the RKKY interaction again but in the short range. The distortion in the square pyramidal coordination, as in $GdCo_{0.27}Sn_{2-\delta}$, appears to help it to achieve that rare disordered configuration. This modified RKKY interaction should lead to a bound triplet state or a ferromagnetic state in the shorter range [39]. If this magnetic interaction could be sustained in the longer range as in the low-Co-doping case, it would lead to a tightly bound singlet state as it should be in the larger AFM matrix in both compositions. A competition between the ferromagnetic interaction and the tendency of the formation of singlet states leads to the GP behavior in $GdCo_{0.27}Sn_{2-\delta}$. A PDOS [Fig. 7(c)] of $GdFeSn_2$ (with pyramidal distortion) very similar to that of $GdCoSn_2$ with distortion [Fig. 7(b)] suggests that the RKKY mechanism gets modified in isostructural $GdFe_{0.17}Sn_{2-\delta}$ too, leading to its GP phase [23].

IV. CONCLUSIONS

To conclude, we found that the $GdM_xSn_{2-\delta}$ (M = Co, Ni, Cu) compounds crystallize in the single phase in the defect $CeNiSi_2$-type crystal structure. All these compounds exhibit long-range AFM ordering at low temperatures. Additionally, $GdCo_{0.27}Sn_{2-\delta}$ also exhibits the GP characteristic below 32 K. Here μ_{eff} estimated from the magnetic susceptibilities in the paramagnetic range was found to be close to that of free Gd^{3+} ions, suggesting the rare-earth ions are the primary contributor to the magnetic property. The frustration parameter $f = |\theta_p|/T_N$, estimated to be in the range of 2.6–3.6, indicates a moderate GFM character. A detailed crystal structure analysis was performed to understand the origin of GP in some members of the $GdM_xSn_{2-\delta}$ (M = Fe, Co, Ni, Cu) series. A slight but very crucial variation was found in the M position of the GP compounds in comparison to that of its non-GP counterparts. Such small variations in the atomic arrangements are found to have a profound effect on the band structure, where M atoms develop tiny magnetic moments in the compounds showing GP behavior. Our study thus establishes that GP behavior in $GdM_xSn_{2-\delta}$ (M = Fe, Co, Ni, Cu) is primarily of structural origin.

ACKNOWLEDGMENTS

K.G. thanks the University Grants Commission (UGC), New Delhi, India, for financial support and T. Das and S. Chatterjee for SEM and EDAX measurements. The work at SINP has been supported through the CMPID-DAE project. M.D.R. acknowledges support and funds from the WB-FIST program of the government of West Bengal, India.

[1] A. M. Pereira, L. Morellon, C. Magen, J. Ventura, P. A. Algarabel, M. R. Ibarra, J. B. Sousa, and J. P. Araújo, Phys. Rev. B **82**, 172406 (2010).

[2] A. Pal, S. N. Shirodkar, S. Gohil, S. Ghosh, U. V. Waghmare, and P. Ayyub, Sci. Rep. **3**, 2051 (2013).

[3] J. Liu, T. Gottschall, K. P. Skokov, J. D. Moore, and O. Gutfleisch, Nat. Mater. **11**, 620 (2012).

[4] V. K. Pecharsky and K. A. Gschneidner, Jr., Adv. Mater. **13**, 683 (2001).

[5] J. Kossut and W. Dobrowolski, Handb. Magn. Mater. **7**, 231 (1993).

[6] R. B. Griffiths, Phys. Rev. Lett. **23**, 17 (1969).
[7] A. J. Bray and M. A. Moore, J. Phys. C **15**, L765 (1982).
[8] R.-F. Yang, Y. Sun, W. He, Q.-A. Li, and Z.-H. Cheng, Appl. Phys. Lett. **90**, 032502 (2007).
[9] W. Jiang, X. Z. Zhou, G. Williams, Y. Mukovskii, and K. Glazyrin, Phys. Rev. Lett. **99**, 177203 (2007).
[10] W. Jiang, X. Z. Zhou, G. Williams, Y. Mukovskii, and K. Glazyrin, Phys. Rev. B **76**, 092404 (2007).
[11] W. Jiang, X. Z. Zhou, G. Williams, Y. Mukovskii, and K. Glazyrin, Phys. Rev. B **77**, 064424 (2008).
[12] J. Deisenhofer, D. Braak, H.-A. Krug von Nidda, J. Hemberger, R. M. Eremina, V. A. Ivanshin, A. M. Balbashov, G. Jug, A. Loidl, T. Kimura, and Y. Tokura, Phys. Rev. Lett. **95**, 257202 (2005).
[13] P. Tong, B. Kim, D. Kwon, T. Qian, S.-I. Lee, S.-W. Cheong, and B. G. Kim, Phys. Rev. B **77**, 184432 (2008).
[14] A. Karmakar, S. Majumdar, S. Kundu, T. K. Nath, and S. Giri, J. Phys.: Condens. Matter **25**, 066006 (2013).
[15] C. Magen, P. A. Algarabel, L. Morellon, J. P. Araújo, C. Ritter, M. R. Ibarra, A. M. Pereira, and J. B. Sousa, Phys. Rev. Lett. **96**, 167201 (2006).
[16] Z. W. Ouyang, V. K. Pecharsky, K. A. Gschneidner, Jr., D. L. Schlagel, and T. A. Lograsso, Phys. Rev. B **74**, 094404 (2006).
[17] Z. W. Ouyang, N. M. Xia, Y. Y. Wu, S. S. Sheng, J. Chen, Z. C. Xia, L. Li, and G. H. Rao, Phys. Rev. B **84**, 054435 (2011).
[18] Z. W. Ouyang, J. Appl. Phys. **108**, 033907 (2010).
[19] B. Malaman and G. Venturini, J. Alloys Compd. **494**, 44 (2010).
[20] O. I. Bodak and E. I. Gladyshevskii, Sov. Phys. Cryst. **14**, 859 (1970).
[21] R. V. Skolozdra, Handb. Phys. Chem. Rare Earths **24**, 399 (1997).
[22] M. Francois, G. Venturini, B. Malaman, and B. Roques, J. Less-Common Met. **160**, 197 (1990).
[23] K. Ghosh, C. Mazumdar, R. Ranganathan, and S. Mukherjee, Sci. Rep. **5**, 15801 (2015).
[24] A. Lindbaum and M. Rotter, Handb. Magn. Mater. **14**, 307 (2002).
[25] J. R. Carvajal, Phys. B (Amsterdam, Neth.) **192**, 55 (1993).
[26] C. P. Sebastian and R. Pöttgen, Monatsh. Chem. **138**, 381 (2007).
[27] S. Baran, F. Henkel, D. Kaczorowski, J. Hernández-Velasco, B. Penc, N. Stüßer, A. Szytula, and E. Wawrzyńska, J. Alloys Compd. **415**, 1 (2006).
[28] A. P. Ramirez, Handb. Magn. Mater. **13**, 423 (2001).
[29] S. M. Zhou, Y. Q. Guo, J. Y. Zhao, L. F. He, and L. Shi, Europhys. Lett. **98**, 57004 (2012).
[30] J. Kumar, S. N. Panja, S. Dengre, and S. Nair, Phys. Rev. B **95**, 054401 (2017).
[31] A. H. Castro Neto, G. Castilla, and B. A. Jones, Phys. Rev. Lett. **81**, 3531 (1998).
[32] M. A. Ruderman and C. Kittel, Phys. Rev. **96**, 99 (1954); T. Kasuya, Prog. Theor. Phys. **16**, 45 (1956); K. Yosida, Phys. Rev. **106**, 893 (1957).
[33] T. Spataru, P. Manfrinetti, A. Palenzona, P. Blaha, M. L. Fornasini, and G. Principi, Intermetallics **10**, 423 (2002).
[34] M. A. Zhuravleva, D. Bilc, R. J. Pcionek, S. D. Mahanti, and M. G. Kanatzidis, Inorg. Chem. **44**, 2177 (2005).
[35] J. P. A. Makongo, N.-T. Suen, S. Guo, S. Saha, R. Greene, J. Paglione, and S. Bobev, J. Solid State Chem. **211**, 95 (2014).
[36] V. I. Anisimov, J. Zaanen, and O. K. Andersen, Phys. Rev. B **44**, 943 (1991); A. I. Lichtenstein, V. I. Anisimov, and J. Zaanen, *ibid.* **52**, 5467(R) (1995).
[37] P. Larson and W. R. L. Lambrecht, Phys. Rev. B **74**, 085108 (2006).
[38] O. K. Andersen, Phys. Rev. B **12**, 3060 (1975).
[39] J. A. Sobota, D. Tanasković, and V. Dobrosavljević, Phys. Rev. B **76**, 245106 (2007).